IEEE Access
Multidisciplinary | Rapid Review | Open Access Journal

SPECIAL SECTION ON EMERGING TRENDS, ISSUES AND CHALLENGES FOR ARRAY SIGNAL PROCESSING AND ITS APPLICATIONS IN SMART CITY

Received December 7, 2019, accepted December 28, 2019, date of publication December 31, 2019, date of current version January 8, 2020.

Digital Object Identifier 10.1109/ACCESS.2019.2963356

Robust and Efficient Adaptive Beamforming Using Nested Subarray Principles

ZHI ZHENG[1,2], (Member, IEEE), TONG YANG[1], DI JIANG[1], AND WEN-QIN WANG[1], (Senior Member, IEEE)

[1]School of Information and Communication Engineering, University of Electronic Science and Technology of China (UESTC), Chengdu 611731, China
[2]Institute of Electronic and Information Engineering in Guangdong, University of Electronic Science and Technology of China (UESTC), Dongguan 523808, China

Corresponding author: Zhi Zheng (zz@uestc.edu.cn)

This work was supported in part by the National Natural Science Foundation of China under Grant 61871086, in part by the Sichuan Science and Technology Program under Grant 2019YJ0191, in part by the Natural Science Foundation of Guangdong Province under Grant 2018A0303130064, and in part by the Fundamental Research Funds for Central Universities of China under Grant 2672018ZYGX2018J003.

ABSTRACT In this paper, we propose an adaptive beamforming algorithm for large uniform linear arrays (ULAs), where only a nested subarray is utilized to calculate the beamforming coefficients for the original ULA. In this algorithm, the steering vectors and powers of the signal-of-interest (SOI) and interferences are firstly estimated using the Capon spatial spectrum and known array structure, and the interference-plus-noise covariance matrix (INCM) is then constructed. Subsequently, an augmented INCM is formed via vectorization and spatial smoothing operations. Finally, the beamformer weight vector is determined by the augmented INCM and the estimated SOI steering vector. Our proposed algorithm exploits the enhanced degrees of freedom of the nested array, and thus can be applied to a large ULA to reduce the implementation complexity. Moreover, it fundamentally eliminates the SOI component. Numerical results demonstrate that the proposed algorithm performs better than the existing approaches.

INDEX TERMS Adaptive beamforming, nested subarray, spatially smoothed matrix (SSM), augmented INCM (AINCM).

I. INTRODUCTION

In array signal processing, adaptive beamforming is a fundamental technology due to wide applications, e.g., in radar, sonar, wireless communications, cognitive radio networks, medical imaging [1]–[3]. The minimum variance distortionless response (MVDR) beamformer is an optimal adaptive filter, which provides outstanding spatial resolution and interference rejection capability [4]. Nevertheless, the standard MVDR beamformer is quite sensitive to the mismatch between the actual steering vector and presumed one, which is caused by various imperfections such as look direction errors and local scattering effects. The standard MVDR beamformer will suffer significant performance deterioration with steering vector mismatches, especially when the training data contains the signal-of-interest (SOI). In the past decades, many robust adaptive beamformers have been suggested to enhance the robustness of the standard MVDR beamformer [5]–[37].

The associate editor coordinating the review of this manuscript and approving it for publication was Liangtian Wan.

Degrees of freedom (DOFs) is a key factor affecting the performance of adaptive beamforming. Generally, a higher number of DOFs means higher spatial resolution and better interference rejection capability [38]. Traditional adaptive beamformers are mostly designed for the uniform linear array (ULA), where the element spacing is not more than half a wavelength to avoid spatial aliasing. However, the number of DOFs of ULAs increases linearly as the number of sensors increases. To enhance the number of DOFs within the ULA configuration, more sensors are required, thus bringing about a high complexity that may be impractical or uneconomical. Fortunately, nonuniform linear arrays (NLAs) provide an effective solution to this issue [39]. By generating the difference coarray [40], a NLA can provide a significantly higher number of DOFs than the traditional ULAs.

The nested array, as a NLA, have attracted intensive attention for years. It can achieve $\mathcal{O}(M^2)$ DOFs using only M physical sensors [41]. In particular, the two-level nested array can yield a hole-free difference coarray. Recently, lots of works have been reported on direction-of-arrival (DOA) estimation based on nested arrays [42]–[50]. But only a few

This work is licensed under a Creative Commons Attribution 4.0 License. For more information, see http://creativecommons.org/licenses/by/4.0/

works on nested array adaptive beamforming are presented. Nested array adaptive beamforming was firstly proposed in [38]. The beamformer of [38] is actually the MVDR beamformer with increased DOFs, where an augmented covariance matrix called spatially smoothed matrix (SSM) is constructed to compute the beamformer weight vector. In [51], another augmented covariance matrix was constructed for adaptive beamforming with enhanced DOFs. The new covariance matrix is obtained by forming a Toeplitz matrix with the observed signal of the virtual array, but it is essentially the square root of the SSM [52]. The beamformers of [38] and [51] do not consider various imperfections such as look direction error and coherent local scattering, and thus they are very sensitive to the model mismatch. To tackle this problem, Yang *et al.* [53] proposed a robust adaptive beamformer, where the interference-plus-noise covariance matrix (INCM) is reconstructed by projecting the SSM into the interference subspace, while the SOI steering vector is estimated by solving a convex optimization problem. The algorithm of [53] is more robust than the methods of [38] and [51] in the presence of various imperfections. However, its performance suffers some degradation as compared to the optimal value, especially at high signal-to-noise ratios (SNRs) because the SOI component is not thoroughly eliminated. These above-mentioned methods utilize the SSM or its derivation to design the adaptive beamformer. However, the SSM needs to take a large number of samples to converge to a full-rank covariance matrix. Accordingly, the resulting beamformers have a slow convergence rate.

In this paper, a novel algorithm based on nested subarray principles is proposed for adaptive beamforming in large-scale ULAs. Unlike the traditional schemes, the proposed algorithm only utilizes a small number of array sensors to determine the weighted vector of the original ULA. Hence, the implementation complexity can be significantly reduced. By constructing an augmented INCM, the proposed algorithm not only exploits the enhanced DOFs of the nested array, but also fundamentally removes the SOI component. Therefore, it achieves better performance than the existing schemes in high SNR regions. Numerical results verify the advantage of the proposed algorithm over the existing algorithms.

The rest of this paper is organized as follows. Some necessary preliminaries including signal model and problem background are described in Section II. An adaptive beamforming algorithm using nested subarrays is suggested in Section III. Numerical examples are provided in Section IV. Finally, conclusions are made in Section V.

Notations: We use bold lower-case and upper-case characters to denote vectors and matrices, respectively. $(\cdot)^T$, $(\cdot)^*$ and $(\cdot)^H$ represent the transpose, complex conjugate and conjugate transpose, respectively. $E\{\cdot\}$ represents the statistical expectation operator, $\|\cdot\|_F$ denotes the Frobenius norm, and vec$(\cdot)$ stands for the vectorization operator that turns a matrix into a vector by stacking all columns on top of the another. $[\cdot]_{i,j}$ denotes the (i,j)th entry of a matrix, and $[\cdot]_i$ denotes the ith element of a vector; diag$(\mathbf{a})$ denotes a diagonal matrix that uses the elements of $\mathbf{a}$ as its diagonal elements. $\mathbf{I}_m$ stands for the $m \times m$ identity matrix, and $\mathbf{0}_{m\times n}$ means the $m \times n$ zero matrix. The symbol $\odot$ denotes the Khatri-Rao product.

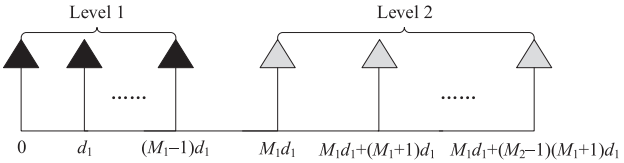

FIGURE 1. The two-level nested array configuration.

II. PRELIMINARIES

A. NESTED ARRAY SIGNAL MODEL AND CONVENTIONAL ADAPTIVE BEAMFORMING

We consider a M-element nested array consisting of two concatenated ULAs as shown in Fig. 1. The inner ULA has M_1 elements with spacing d_1, and the outer ULA has M_2 elements with spacing $d_2 = (M_1 + 1)d_1$. The element spacing d_1 is generally set to $\lambda/2$, where λ denotes the carrier wavelength. More accurately, the sensor positions are $z_i d_1$, where z_i belongs to an integer set $\mathbb{S} = \{z_i, i = 1, 2, \ldots, M\} = \{0, 1, \ldots, M_1 - 1, M_1, 2(M_1 + 1) - 1, \ldots, M_2(M_1 + 1) - 1\}$. Suppose that one SOI and L interference signals impinge on the nested array from the distinct directions $\theta_1, \ldots, \theta_N$. The array observed vector at time instant k is given by

$$\mathbf{x}(k) = \mathbf{x}_s(k) + \mathbf{x}_i(k) + \mathbf{x}_n(k) \tag{1}$$

where $\mathbf{x}_s(k) = \mathbf{a}_0 s_0(k)$, $\mathbf{x}_i(k) = \sum_{l=1}^{L} \mathbf{a}_l s_l(k)$, and $\mathbf{x}_n(k)$ are the SOI, interference, and noise components, respectively. Moreover, these components are assumed to be mutually independent. $s_l(k)$ is the lth source signal waveform, and $\mathbf{a}_l = \mathbf{a}(\theta_l)$ is the corresponding steering vector. $\mathbf{x}_n(k)$ is assumed to be the additive spatially white Gaussian noise with zero mean and variance σ_n^2. The steering vector for the lth source is expressed as

$$\mathbf{a}(\theta_l) = \left[1, e^{j\frac{2\pi}{\lambda} z_2 d_1 \sin\theta_l}, \ldots, e^{j\frac{2\pi}{\lambda} z_M d_1 \sin\theta_l}\right]^T. \tag{2}$$

The beamformer output is given by

$$y(k) = \mathbf{w}^H \mathbf{x}(k) \tag{3}$$

where $\mathbf{w} = [w_1, \ldots, w_M]^T \in \mathbb{C}^{M\times 1}$ is the beamformer weight vector. The output signal-to-interference-plus-noise ratio (SINR) of the beamformer is defined as

$$\text{SINR} = \frac{\sigma_0^2 |\mathbf{w}^H \mathbf{a}_0|^2}{\mathbf{w}^H \mathbf{R}_{i+n} \mathbf{w}} \tag{4}$$

where $\sigma_0^2 = E\{|s_0(k)|^2\}$ is the SOI power, and $\mathbf{R}_{i+n}$ is the $M \times M$ INCM, whose definition is given by

$$\begin{aligned} \mathbf{R}_{i+n} &= E\left\{(\mathbf{x}_i(k) + \mathbf{x}_n(k))(\mathbf{x}_i(k) + \mathbf{x}_n(k))^H\right\} \\ &= \sum_{l=1}^{L} \sigma_l^2 \mathbf{a}_l \mathbf{a}_l^H + \sigma_n^2 \mathbf{I}_M \end{aligned} \tag{5}$$

where σ_l^2 denotes the lth interference power.

Maximizing the output SINR (4) is equivalent to the minimization problem:

$$\min_{\mathbf{w}} \mathbf{w}^H \mathbf{R}_{i+n} \mathbf{w} \quad \text{s.t.} \quad \mathbf{w}^H \mathbf{a}_0 = 1, \tag{6}$$

whose solution is

$$\mathbf{w}_{\text{opt}} = \frac{\mathbf{R}_{i+n}^{-1} \mathbf{a}_0}{\mathbf{a}_0^H \mathbf{R}_{i+n}^{-1} \mathbf{a}_0}. \tag{7}$$

Since the exact $\mathbf{R}_{i+n}$ is unavailable in practice, it is usually replaced by the sample covariance matrix (SCM):

$$\hat{\mathbf{R}}_{\mathbf{xx}} = \frac{1}{K} \sum_{k=1}^{K} \mathbf{x}(k) \mathbf{x}^H(k) \tag{8}$$

where K denotes the number of training snapshots. Then the resulting beamformer is

$$\mathbf{w}_{\text{SMI}} = \frac{\hat{\mathbf{R}}_{\mathbf{xx}}^{-1} \mathbf{a}_0}{\mathbf{a}_0^H \hat{\mathbf{R}}_{\mathbf{xx}}^{-1} \mathbf{a}_0}, \tag{9}$$

which is the so-called sample matrix inversion (SMI) beamformer.

B. ADAPTIVE BEAMFORMING WITH ENHANCED DOFS

To exploit the enhanced DOFs of the nested array, some approaches, such as [51], construct an augmented covariance matrix using the coarray output, and further generate the weighted vector of the beamformer. However, the dimension of the generated weighted vector is more than that of the physical array. Therefore, the adaptive beamforming with enhanced DOFs can only be applied to a large array to reduce the implementation complexity.

The covariance matrix of $\mathbf{x}(k)$ is expressed as

$$\mathbf{R}_{\mathbf{xx}} = E\{\mathbf{x}(k)\mathbf{x}^H(k)\} = \mathbf{A}\Lambda\mathbf{A}^H + \sigma_n^2 \mathbf{I}_M \tag{10}$$

where $\Lambda = E\{\mathbf{s}(t)\mathbf{s}^H(t)\} = \text{diag}([\sigma_0^2, \sigma_1^2, \ldots, \sigma_L^2])$ is the signal covariance matrix.

Vectorizing $\mathbf{R}_{\mathbf{xx}}$ yields

$$\mathbf{z} = \text{vec}(\mathbf{R}_{\mathbf{xx}}) = (\mathbf{A}^* \odot \mathbf{A})\mathbf{p} + \sigma_n^2 \vec{\mathbf{1}}_n \tag{11}$$

where $\mathbf{p} = [\sigma_0^2, \sigma_1^2, \ldots, \sigma_L^2]^T$, and $\vec{\mathbf{1}}_n = [\mathbf{e}_1^T, \mathbf{e}_2^T, \ldots, \mathbf{e}_M^T]^T$ with $\mathbf{e}_i$ being a column vector of all zeros except one 1 at the ith location. The vector $\mathbf{z}$ can be regarded as a single snapshot data from the equivalent signal vector $\mathbf{p}$, and $\sigma_n^2 \vec{\mathbf{1}}_n$ is a deterministic noise vector. The distinct rows of $\mathbf{A}^* \odot \mathbf{A}$ correspond to the manifold of a longer array whose sensor locations are represented by the difference set of $\mathbb{S}$.

Removing the redundant rows from the vector $\mathbf{z}$ and rearranging the remaining rows gives [41]:

$$\mathbf{z}_1 = \mathbf{A}_1 \mathbf{p} + \sigma_n^2 \vec{\mathbf{e}}' \tag{12}$$

where $\mathbf{A}_1 \in \mathbb{C}^{(2M_2(M_1+1)-1)\times(L+1)}$ is a manifold matrix, which is constructed by removing the repeated rows from $\mathbf{A}^* \odot \mathbf{A}$ and rearranging the remaining rows, and $\vec{\mathbf{e}}' \in \mathbb{R}^{(2M_2(M_1+1)-1)\times 1}$ means an all-zero vector except one 1 at the $M_2(M_1+1)$th location.

Dividing $\mathbf{z}_1$ into $M_2(M_1+1)$ subvectors, we can construct the following full-rank matrix [41]:

$$\mathbf{R}_{\mathbf{ss}} = \frac{1}{M_2(M_1+1)} \sum_{i=1}^{M_2(M_1+1)} \mathbf{z}_{1i} \mathbf{z}_{1i}^H \tag{13}$$

where $\mathbf{z}_{1i}$ is the ith subvector corresponding to the $(M_2(M_1+1)-i+1)$th to $(2M_2(M_1+1)-i)$th rows of $\mathbf{z}_1$.

The matrix $\mathbf{R}_{\mathbf{ss}}$ can be represented as [41]:

$$\mathbf{R}_{\mathbf{ss}} = \frac{1}{M_2(M_1+1)} \tilde{\mathbf{R}}^2 \tag{14}$$

where

$$\tilde{\mathbf{R}} = \mathbf{A}_{11} \Lambda \mathbf{A}_{11}^H + \sigma_n^2 \mathbf{I}_{\tilde{M}} \tag{15}$$

appears the same form as the covariance matrix of the observed signal from a longer ULA with $M_2(M_1+1)$ elements, whose manifold matrix is denoted by $\mathbf{A}_{11}$ consisting of the last $M_2(M_1+1)$ rows of $\mathbf{A}_1$. Therefore, the matrix $\tilde{\mathbf{R}}$, also referred to as the SSM, can be used to perform adaptive beamforming.

Employing the matrix $\tilde{\mathbf{R}}$, the adaptive beamformer with enhanced DOFs is given by [51]:

$$\mathbf{w} = \frac{\tilde{\mathbf{R}}^{-1} \mathbf{d}(\theta_0)}{\mathbf{d}^H(\theta_0) \tilde{\mathbf{R}}^{-1} \mathbf{d}(\theta_0)} \tag{16}$$

where $\mathbf{d}(\theta_0)$ denotes the SOI steering vector of an equivalent ULA with $M_2(M_1+1)$ elements. However, the adaptive beamformer is very sensitive to the model mismatch and has a slow convergence rate.

III. PROPOSED ALGORITHM

In this section, we utilize the nested array to develop a new adaptive beamforming algorithm with enhanced DOFs. Unlike the existing schemes, our algorithm not only exploits the enhanced DOFs of nested arrays, but also thoroughly removes the SOI component.

First, we construct the INCM of the nested array via steering vector and power estimation. With the known array structure, the steering vectors of the incident signals can be uniquely determined by their DOAs. When the number of signals is unknown, we utilize the Capon spatial spectrum to estimate the DOAs of the SOI and interferences. The Capon spectrum estimator is [54]:

$$\hat{P}(\theta) = \frac{1}{\mathbf{a}^H(\theta) \hat{\mathbf{R}}_{\mathbf{xx}}^{-1} \mathbf{a}(\theta)} \tag{17}$$

where $\mathbf{a}(\theta)$ is the steering vector associated with a direction $\theta \in [-90°, 90°]$. From (17), we can get multiple peaks. Since there may be some spurious peaks, the number of the peaks is usually greater than the number of sources. Using the minimum eigenvalue of $\hat{\mathbf{R}}_{\mathbf{xx}}$ as the threshold, we can eliminate most of the spurious peaks. Assume there are still $L'+1$ peaks above the threshold, we can derive the corresponding DOA estimates, $\hat{\theta}_0, \hat{\theta}_1, \ldots, \hat{\theta}_{L'}$ by the positions of the peaks. Further, we can determine the DOAs of the SOI and

interferences from different angular sectors. As [18], [53], we have assumed that Θ is the angular sector in which the SOI lies and $\bar{\Theta}$ is the out-of-sector of Θ. Suppose that $\hat{\theta}_0$ is located at Θ, while $\hat{\theta}_1, \ldots, \hat{\theta}_{L'}$ belong to $\bar{\Theta}$. Then, the estimates of interference steering vectors, $\mathbf{a}(\hat{\theta}_1), \mathbf{a}(\hat{\theta}_2), \ldots, \mathbf{a}(\hat{\theta}_{L'})$, can be obtained using the known array geometry and the estimated DOAs. Additionally, the interference powers can be estimated as $P(\hat{\theta}_1), P(\hat{\theta}_2), \ldots, P(\hat{\theta}_{L'})$.

The INCM of the nested array is reconstructed as

$$\hat{\mathbf{R}}_{i+n} = \sum_{l=1}^{L'} P(\hat{\theta}_l)\mathbf{a}(\hat{\theta}_l)\mathbf{a}^H(\hat{\theta}_l) + \hat{\sigma}_n^2\mathbf{I}_M \tag{18}$$

where $\hat{\sigma}_n^2$ is the estimate of the noise variance, which is computed as the minimum eigenvalue of $\hat{\mathbf{R}}_{\mathbf{xx}}$.

Again, we vectorize $\hat{\mathbf{R}}_{i+n}$ to get the following vector

$$\hat{\mathbf{y}} = \mathrm{vec}(\hat{\mathbf{R}}_{i+n}) = (\hat{\mathbf{A}}^* \odot \hat{\mathbf{A}})\hat{\mathbf{p}} + \hat{\sigma}_n^2\vec{\mathbf{1}}_n \tag{19}$$

where

$$\hat{\mathbf{p}} = [P(\hat{\theta}_1), P(\hat{\theta}_2), \ldots, P(\hat{\theta}_{L'})]. \tag{20}$$

Removing the redundant rows from $\hat{\mathbf{y}}$ and rearranging them to form a new vector $\hat{\mathbf{y}}_1$ expressed as

$$\hat{\mathbf{y}}_1 = \hat{\mathbf{A}}_1\hat{\mathbf{p}} + \hat{\sigma}_n^2\vec{\mathbf{e}}' \tag{21}$$

where $\hat{\mathbf{A}}_1 \in \mathbb{C}^{(2M_2(M_1+1)-1)\times L'}$ is a manifold matrix corresponding to the virtual ULA.

From the vector $\hat{\mathbf{y}}_1$, we construct the following Toeplitz matrix [52]:

$$\bar{\mathbf{R}} = \begin{bmatrix} [\hat{\mathbf{y}}_1]_{\bar{M}} & [\hat{\mathbf{y}}_1]_{\bar{M}-1} & \cdots & [\hat{\mathbf{y}}_1]_1 \\ [\hat{\mathbf{y}}_1]_{\bar{M}+1} & [\hat{\mathbf{y}}_1]_{\bar{M}} & \cdots & [\hat{\mathbf{y}}_1]_2 \\ \vdots & \vdots & \ddots & \vdots \\ [\hat{\mathbf{y}}_1]_{2\bar{M}-1} & [\hat{\mathbf{y}}_1]_{2\bar{M}-2} & \cdots & [\hat{\mathbf{y}}_1]_{\bar{M}} \end{bmatrix} \tag{22}$$

where $\bar{M} = M_2(M_1+1)$, and the matrix $\bar{\mathbf{R}}$ is known as the augmented INCM (AINCM).

Theorem 1: The matrix $\bar{\mathbf{R}}$ can be further expressed as

$$\bar{\mathbf{R}} = \hat{\mathbf{A}}_{11}\hat{\Lambda}\hat{\mathbf{A}}_{11}^H + \hat{\sigma}_n^2\mathbf{I}_{\bar{M}}. \tag{23}$$

where

$$\hat{\mathbf{A}}_{11} = [\mathbf{d}(\hat{\theta}_1), \mathbf{d}(\hat{\theta}_2), \ldots, \mathbf{d}(\hat{\theta}_{L'})], \tag{24}$$

$$\mathbf{d}(\hat{\theta}_l) = [v_l^0, v_l^1, \ldots, v_l^{\bar{M}-1}]^T, \tag{25}$$

$$\hat{\Lambda} = \mathrm{diag}[P(\hat{\theta}_1), P(\hat{\theta}_2), \ldots, P(\hat{\theta}_{L'})]. \tag{26}$$

Proof: According to (22), the matrix $\bar{\mathbf{R}}$ can be written as

$$\begin{aligned} \bar{\mathbf{R}} &= [\mathbf{J}_0\hat{\mathbf{y}}_1, \mathbf{J}_1\hat{\mathbf{y}}_1, \ldots, \mathbf{J}_{\bar{M}-1}\hat{\mathbf{y}}_1] \\ &= [\mathbf{J}_0\hat{\mathbf{A}}_1\hat{\mathbf{p}} + \mathbf{J}_0\hat{\sigma}_n^2\vec{\mathbf{e}}', \mathbf{J}_1\hat{\mathbf{A}}_1\hat{\mathbf{p}} + \mathbf{J}_1\hat{\sigma}_n^2\vec{\mathbf{e}}', \\ &\qquad \ldots, \mathbf{J}_{\bar{M}-1}\hat{\mathbf{A}}_1\hat{\mathbf{p}} + \mathbf{J}_{\bar{M}-1}\hat{\sigma}_n^2\vec{\mathbf{e}}'] \\ &= [\mathbf{J}_0\hat{\mathbf{A}}_1\hat{\mathbf{p}}, \mathbf{J}_1\hat{\mathbf{A}}_1\hat{\mathbf{p}}, \ldots, \mathbf{J}_{\bar{M}-1}\hat{\mathbf{A}}_1\hat{\mathbf{p}}] \\ &\quad + [\mathbf{J}_0\hat{\sigma}_n^2\vec{\mathbf{e}}', \mathbf{J}_1\hat{\sigma}_n^2\vec{\mathbf{e}}', \ldots, \mathbf{J}_{\bar{M}-1}\hat{\sigma}_n^2\vec{\mathbf{e}}'] \\ &= [\mathbf{J}_0\hat{\mathbf{A}}_1\hat{\mathbf{p}}, \mathbf{J}_1\hat{\mathbf{A}}_1\hat{\mathbf{p}}, \ldots, \mathbf{J}_{\bar{M}-1}\hat{\mathbf{A}}_1\hat{\mathbf{p}}] + \hat{\sigma}_n^2\mathbf{I}_{\bar{M}} \end{aligned} \tag{27}$$

where

$$\mathbf{J}_i = [\mathbf{0}_{\bar{M}\times(\bar{M}-1-i)}, \mathbf{I}_{\bar{M}}, \mathbf{0}_{\bar{M}\times i}] \tag{28}$$

$$\hat{\mathbf{A}}_1 = [\hat{\mathbf{a}}_{11}, \hat{\mathbf{a}}_{12}, \ldots, \hat{\mathbf{a}}_{1L'}] \tag{29}$$

with

$$\hat{\mathbf{a}}_{1l} = [v_l^{-\bar{M}+1}, v_l^{-\bar{M}+2}, \ldots, v_l^0, \ldots, v_l^{\bar{M}-1}]^T. \tag{30}$$

On the other hand, we have

$$\hat{\mathbf{A}}_{11}\hat{\Lambda}\hat{\mathbf{A}}_{11}^H + \hat{\sigma}_n^2\mathbf{I}_{\bar{M}} = \sum_{l=1}^{L'} P(\hat{\theta}_l)\mathbf{d}(\hat{\theta}_l)\mathbf{d}^H(\hat{\theta}_l) + \hat{\sigma}_n^2\mathbf{I}_{\bar{M}}. \tag{31}$$

Therefore, (23) is equivalent to

$$[\mathbf{J}_0\hat{\mathbf{A}}_1\hat{\mathbf{p}}, \mathbf{J}_1\hat{\mathbf{A}}_1\hat{\mathbf{p}}, \ldots, \mathbf{J}_{\bar{M}-1}\hat{\mathbf{A}}_1\hat{\mathbf{p}}] = \sum_{l=1}^{L'} P(\hat{\theta}_l)\mathbf{d}(\hat{\theta}_l)\mathbf{d}^H(\hat{\theta}_l). \tag{32}$$

Namely, we only need to prove:

$$[\mathbf{J}_0\hat{\mathbf{A}}_1\hat{\mathbf{p}}, \mathbf{J}_1\hat{\mathbf{A}}_1\hat{\mathbf{p}}, \ldots, \mathbf{J}_{\bar{M}-1}\hat{\mathbf{A}}_1\hat{\mathbf{p}}]_{i,j} = \left[\sum_{l=1}^{L'} P(\hat{\theta}_l)\mathbf{d}(\hat{\theta}_l)\mathbf{d}^H(\hat{\theta}_l)\right]_{i,j}. \tag{33}$$

The left-hand side of (33) can be expressed as

$$\begin{aligned} &[\mathbf{J}_0\hat{\mathbf{A}}_1\hat{\mathbf{p}}, \mathbf{J}_1\hat{\mathbf{A}}_1\hat{\mathbf{p}}, \ldots, \mathbf{J}_{\bar{M}-1}\hat{\mathbf{A}}_1\hat{\mathbf{p}}]_{i,j} \\ &= \left[\mathbf{J}_{j-1}\hat{\mathbf{A}}_1\hat{\mathbf{p}}\right]_i = \left[\sum_{l=1}^{L'} P(\hat{\theta}_l)\mathbf{J}_{j-1}\hat{\mathbf{a}}_{1l}\right]_i \\ &= \left[\sum_{l=1}^{L'} P(\hat{\theta}_l)[v_l^{1-j}, v_l^{2-j}, \ldots, v_l^{\bar{M}-j}]^T\right]_i \\ &= \sum_{l=1}^{L'} P(\hat{\theta}_l)v_l^{i-j} \end{aligned} \tag{34}$$

where $v_l = e^{-j\frac{2\pi}{\lambda}d_1\sin(\hat{\theta}_l)}$.

The right-hand side of (33) can be expressed as

$$\begin{aligned} \left[\sum_{l=1}^{L'} P(\hat{\theta}_l)\mathbf{d}(\hat{\theta}_l)\mathbf{d}^H(\hat{\theta}_l)\right]_{i,j} &= \sum_{l=1}^{L'} P(\hat{\theta}_l)[\mathbf{d}(\hat{\theta}_l)\mathbf{d}^H(\hat{\theta}_l)]_{i,j} \\ &= \sum_{l=1}^{L'} P(\hat{\theta}_l)[\mathbf{d}(\hat{\theta}_l)]_i[\mathbf{d}^H(\hat{\theta}_l)]_j \\ &= \sum_{l=1}^{L'} P(\hat{\theta}_l)v_l^{i-j}. \end{aligned} \tag{35}$$

Comparing (34) and (35) results in (33). Consequently, the following equation holds:

$$\bar{\mathbf{R}} = \hat{\mathbf{A}}_{11}\hat{\Lambda}\hat{\mathbf{A}}_{11}^H + \hat{\sigma}_n^2\mathbf{I}_{\bar{M}}. \tag{36}$$

□

Algorithm 1 Proposed Adaptive Beamforming

1: Create the Capon spatial spectrum based on the given nested subarray.
2: Estimate the DOAs of the SOI and interferences via peak searching, and derive the steering vectors and powers of the interferences.
3: Reconstruct the INCM $\hat{\mathbf{R}}_{i+n}$ using (18).
4: Vectorize $\hat{\mathbf{R}}_{i+n}$ to yield the vector $\hat{\mathbf{y}}$, remove the redundant rows from $\hat{\mathbf{y}}$ and rearrange the remaining rows to generate a new vector $\hat{\mathbf{y}}_1$.
5: Construct the AINCM $\bar{\mathbf{R}}$ using (22).
6: Calculate the steering vector $\mathbf{d}(\hat{\theta}_0)$ of an $\bar{M}$-element ULA with the estimated SOI DOA $\hat{\theta}_0$.
7: Substitute $\bar{\mathbf{R}}$ and $\mathbf{d}(\hat{\theta}_0)$ into (16) to result in the proposed beamformer (38).

To design the adaptive beamformer with enhanced DOFs, we need to consider an $\bar{M}$-element equivalent ULA. With the estimated SOI DOA $\hat{\theta}_0$, the SOI steering vector corresponding to the large ULA is given by

$$\mathbf{d}(\hat{\theta}_0) = \left[1, e^{j\frac{2\pi}{\lambda}2d_1\sin\hat{\theta}_0}, \ldots, e^{j\frac{2\pi}{\lambda}(\bar{M}-1)d_1\sin\hat{\theta}_0}\right]^T. \quad (37)$$

Substituting $\bar{\mathbf{R}}$ and $\mathbf{d}(\hat{\theta}_0)$ in (16), we get a new adaptive beamformer whose weight vector is

$$\mathbf{w}_{\text{pro}} = \frac{\bar{\mathbf{R}}^{-1}\mathbf{d}(\hat{\theta}_0)}{\mathbf{d}^H(\hat{\theta}_0)\bar{\mathbf{R}}^{-1}\mathbf{d}(\hat{\theta}_0)}. \quad (38)$$

For clarity, the proposed algorithm is summarized in Algorithm 1.

Remark 1: Unlike the traditional methods, the proposed approach is used for implementing low-complexity beamforming in large-scale array systems. Specifically, for a large ULA, our algorithm only selects a small number of sensors to form a nested subarray, and uses its coarray output to generate an augmented weighted vector. Then, the generated augmented weighted vector is applied to the whole ULA to realize beamforming. By doing so, the full aperture of the original ULA can be exploited, while the implementation complexity of beamforming is significantly reduced.

Remark 2: For an $\bar{M}$-element ULA, the proposed algorithm only utilizes M sensors to calculate the beamforming coefficients for the original ULA. The required multiplications are $\mathcal{O}(\max(M^2S, M^3))$, where S denotes the number of grid points in the angular sector. By comparison, the traditional schemes require a complexity of $\mathcal{O}(\max(\bar{M}^2S, \bar{M}^3))$ with $\bar{M} > M$, because all the sensors are utilized to calculate the beamforming coefficients. Evidently, our algorithm has a lower complexity than the traditional schemes because it requires lower dimensional matrix calculations.

IV. NUMERICAL EXAMPLES

In this section, numerical examples are provided to investigate the performance of the proposed algorithm. In all the examples, we consider a ULA with $M = 12$ sensors and element spacing $\lambda/2$, and choose a two-level nested array ($M_1 = M_2 = 3$) as the sampling subarray of our proposed beamformer and the beamformers [51], [53]. One SOI is presumed to arrive at the array from the direction $\theta_0 = 0°$. Three interferences are assumed to arrive at the array from the directions $-30°$, $30°$ and $45°$, respectively. The INR is fixed at 30 dB in all examples. The input SNR is fixed at 20 dB (except the cases where the SNR varies), while the number of snapshots is set as $K = 100$ (except the cases where the number of snapshots varies). For each scenario, 500 Monte Carlo trials are performed.

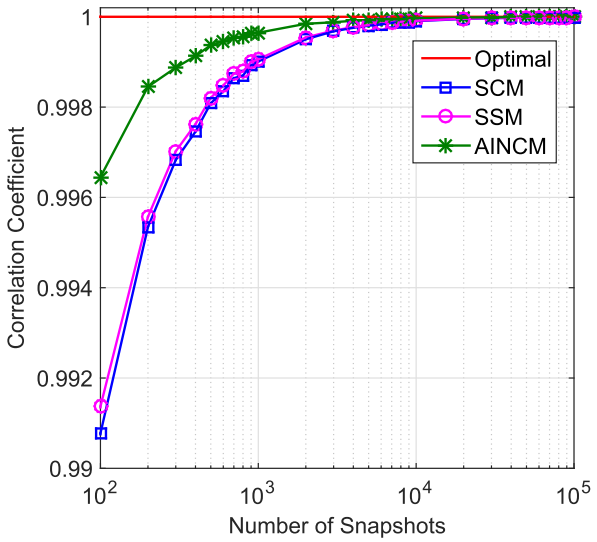

FIGURE 2. Correlation coefficients of SCM, SSM and AINCM versus the number of snapshots.

A. CONVERGENCE RATES OF COVARIANCE MATRICES

In the first experiment, we examine the convergence rates of the SCM, SSM and AINCM. To evaluate the similarity between two matrices, we introduce the following correlation coefficient:

$$cor(\hat{\mathbf{R}}, \mathbf{R}) = \frac{|\text{vec}^H(\hat{\mathbf{R}})\text{vec}(\mathbf{R})|}{\|\text{vec}(\hat{\mathbf{R}})\|_F\|\text{vec}(\mathbf{R})\|_F} \quad (39)$$

where $\mathbf{R}$ and $\hat{\mathbf{R}}$ denote the true matrix and the estimated matrix, respectively. Clearly, when $cor(\hat{\mathbf{R}}, \mathbf{R})$ is closer to 1, the similarity between $\hat{\mathbf{R}}$ and $\mathbf{R}$ is higher.

Fig. 2 shows the correlation coefficients of the covariance matrices versus number of snapshots, while Fig. 3 displays the correlation coefficients of their inverse matrices versus number of snapshots. It is observed that the convergence rate of the AINCM is obviously faster than those of the SCM and the SSM, and the latter two converge to their theoretical values only when $K > 10^4$. On the other hand, we see clearly from Fig. 3 that the inverse of the AINCM also shows a faster convergence rate than that of the SCM, and especially that of the SSM, which still cannot converge to its theoretical value even when $K = 10^5$. It can be attributed to the fact that the AINCM can be expressed as the covariance matrix form (23),

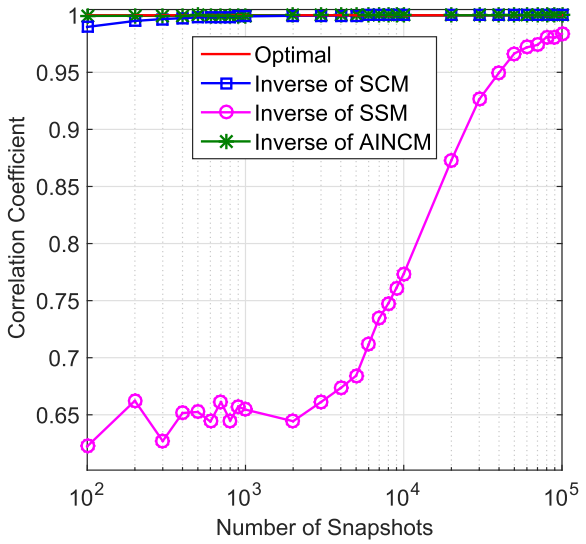

FIGURE 3. Correlation coefficients of the inverses of SCM, SSM and AINCM versus the number of snapshots.

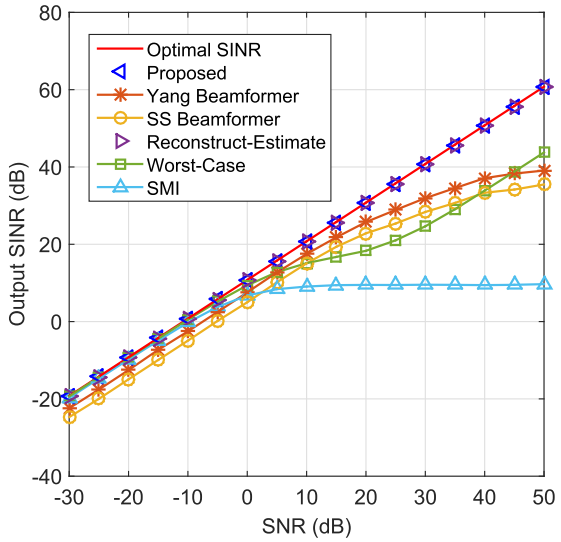

FIGURE 4. Output SINR versus the SNR at $K = 100$ and INR = 30 dB. First example.

and its model error is only determined by the accuracy of DOA and power estimates.

B. OUTPUT SINRS OF BEAMFORMERS

In the second experiment, we compare the proposed beamformer with the following adaptive beamformers: *i*) Yang beamformer [53]; *ii*) SS beamformer [51]; *iii*) reconstruct-estimate-based beamformer [18]; *iv*) worst-case-based beamformer [7]; *v*) SMI beamformer. For the beamformers of [18], [53] and our proposed beamformer, the angular sector of the SOI is assumed to be $\Theta = [-5°, 5°]$, while the complement sector of Θ is $\bar{\Theta} = [-90°, -5°) \cup (5°, 90°]$. The factor ε is set to $\varepsilon = 0.3\bar{M}$ in the worst-case-based beamformer. The Matlab CVX toolbox [55] is utilized for solving these convex optimization problems in [7], [18], [53].

1) EXAMPLE 1—EXACTLY KNOWN SIGNAL STEERING VECTOR

Firstly, we consider the situation where the steering vectors of the SOI and interferences are accurately known. It is noteworthy that even in the absence of steering vector mismatches, the SOI component contained in the training data can seriously slow down the convergence rates of adaptive beamformers. The output SINR of the examined beamformers versus input SNR is shown in Fig. 4, from which we see that the proposed beamformer achieves almost the same performance as the reconstruct-estimate-based beamformer [18]. The two beamformers provide nearly optimal SINR from -30 dB to 50 dB and significantly outperform the remaining beamformers at high SNRs because the SOI component is thoroughly eliminated. However, the proposed algorithm is computationally more efficient than [18] because it uses fewer sensors to calculate the weight vector as [51], [53]. The output SINR of the beamformers against the snapshot number is plotted in Fig. 5. It is observed that both the proposed

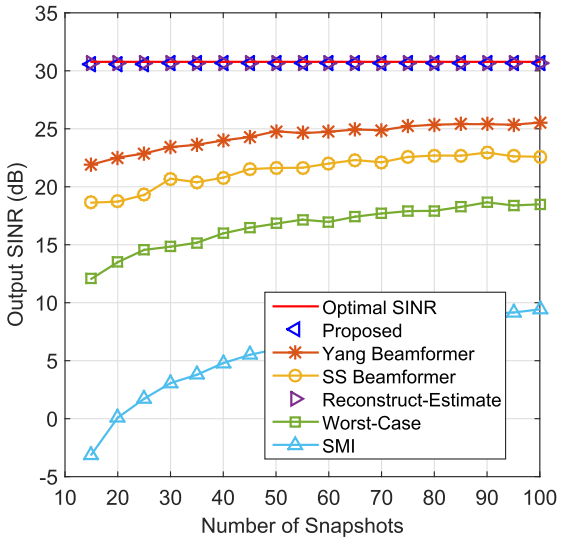

FIGURE 5. Output SINR versus the number of snapshots at SNR = 20 dB and INR = 30 dB. First example.

beamformer and the beamformer of [18] enjoy a much faster convergence rate than the other beamformers because the convergence properties of the INCM and the AINCM are distinctly better than those of the SCM and the SSM.

2) EXAMPLE 2—SIGNAL LOOK DIRECTION MISMATCH

Secondly, the influence of signal look direction error on performance of the proposed beamformer is examined. The direction errors of the SOI and the interferences are uniformly distributed in $[-4°, 4°]$. Namely, the true direction of the SOI is uniformly distributed in $[-4°, 4°]$, and the distribution intervals of the interferences are $[-34°, -26°]$, $[26°, 34°]$ and $[41°, 49°]$, respectively. Note that the directions of the SOI and the interferences vary in each trial while keeping unchanged from snapshot to snapshot. Fig. 6 depicts the

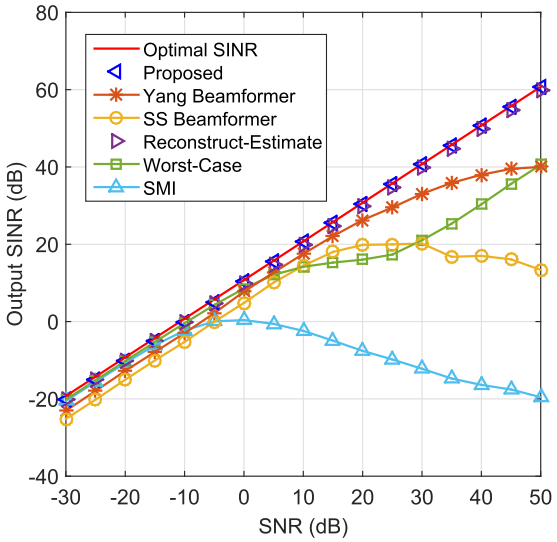

FIGURE 6. Output SINR versus the SNR at $K = 100$ and INR $= 30$ dB. Second example.

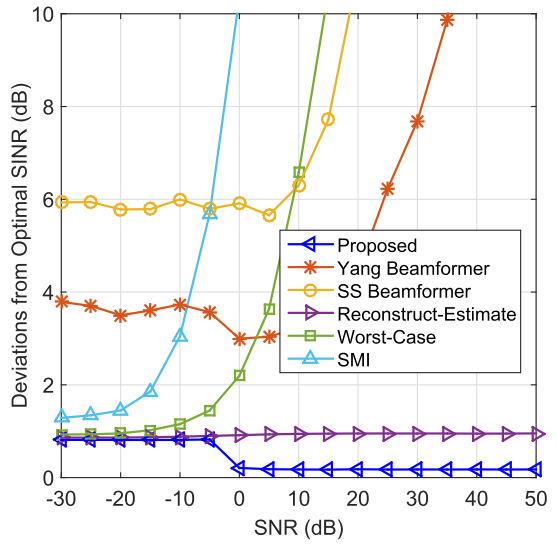

FIGURE 7. Deviations from optimal SINR versus the SNR at $K = 100$ and INR $= 30$ dB. Second example.

output SINR of the examined beamformers versus SNR. But there is still a slight gap between some beamformers and the optimal SINR, as shown in Fig. 7. It is observed that the proposed beamformer and the reconstruct-estimate-based beamformer [18] have similar output performance, and both of them perform better than the remaining beamformers at high SNRs. Moreover, the proposed beamformer achieves about 1 dB gain over the beamformer of [18] when the SNR is more than 0 dB. The output SINR of the examined beamformers against number of snapshots is illustrated in Fig. 8. It can be seen that the proposed beamformer and the beamformer of [18] achieve almost the same and fast convergence rate, while the other beamformers experience a slow convergence rate.

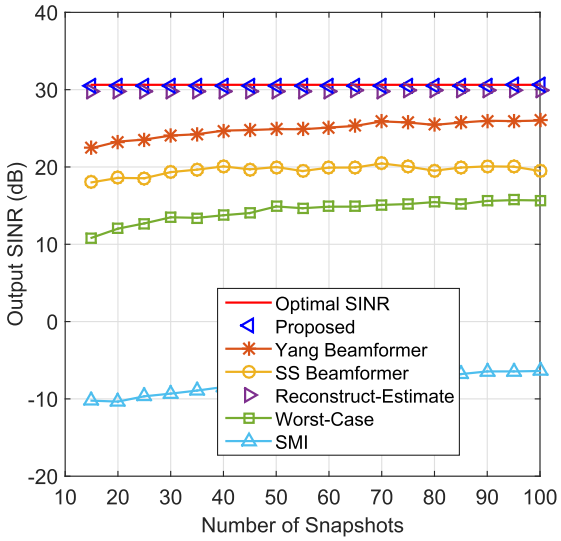

FIGURE 8. Output SINR versus the number of snapshots at SNR $= 20$ dB and INR $= 30$ dB. Second example.

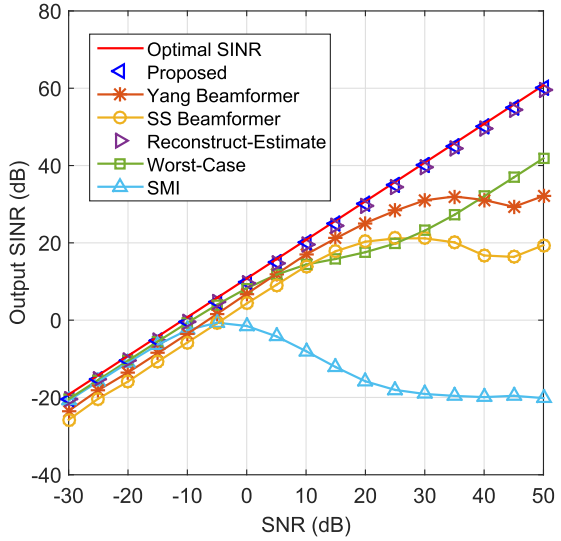

FIGURE 9. Output SINR versus the SNR at $K = 100$ and INR $= 30$ dB. Third example.

3) EXAMPLE 3—SOI STEERING VECTOR MISMATCH DUE TO COHERENT LOCAL SCATTERING

Thirdly, the SOI steering vector is affected by coherent local scattering effects and expressed as [7]:

$$\mathbf{a}_0 = \mathbf{p} + \sum_{p=1}^{4} e^{j\psi_p}\mathbf{a}(\theta_p) \tag{40}$$

where $\mathbf{p}$ corresponds to the direct path while $\mathbf{a}(\theta_p)$ $(p = 1, 2, 3, 4)$ refers to the coherently scattered paths. The angles θ_p $(p = 1, 2, 3, 4)$ are independently and uniformly distributed in $[\theta_0 - 4°, \theta_0 + 4°]$ in each trial. The phase parameters ψ_p $(p = 1, 2, 3, 4)$ are independently and uniformly drawn from $[0, 2\pi]$ in each trial. Note that θ_p and ψ_p change from trial to trial while keeping unchanged from snapshot to snapshot. Fig. 9 demonstrates the output SINR of the

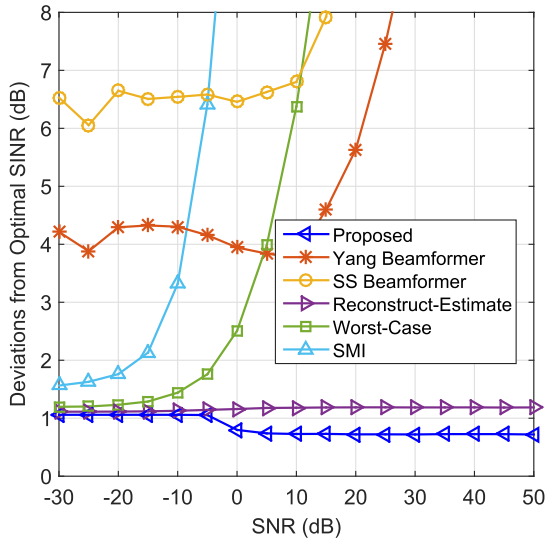

FIGURE 10. Deviations from optimal SINR versus the SNR at $K = 100$ and INR = 30 dB. Third example.

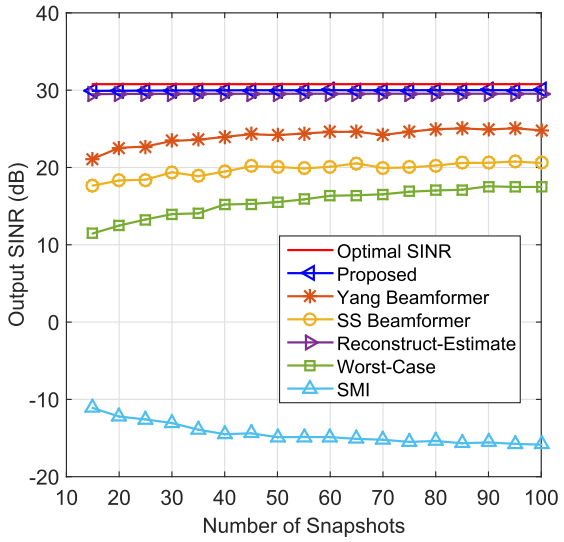

FIGURE 11. Output SINR versus the number of snapshots at SNR = 20 dB and INR = 30 dB. Third example.

examined beamformers versus the SNR. Their deviations from the optimal SINR are displayed in Fig. 10. Note that in this example, the SNR is defined by considering all signal scattering paths. As it can be observed, the proposed beamformer and the reconstruct-estimate-based beamformer [18] achieve almost the same output SINR, and they are superior to the remaining beamformers. More specifically, when the SNR is greater than -5 dB, the proposed beamformer performs better than [18] because it eliminates the SOI component and gets a more accurate INCM. When the SNR is greater than -5 dB, there is about 1 dB performance loss for the beamformer of [18] and our proposed beamformer, because there may be no obvious peak in Θ for the Capon spectrum and the presumed DOA is used to derive the SOI steering vector. The output SINR of the examined beamformers against number of snapshots is shown in Fig. 11. We observe clearly that our proposed beamformer and the beamformer of [18] show significantly better convergence performance than other beamformers being compared.

V. CONCLUSION

In this paper, we have developed a new adaptive beamforming approach for large-scale ULAs based on nested subarray principles. Typically, the proposed method is applied to a large ULA to reduce the implementation complexity. Compared with the existing methods, our approach not only exploits the enhanced DOFs of the nested array, but also thoroughly removes the SOI component. Therefore, its performance is more stable in the presence of various non-ideal factors. Numerical results show that our proposed approach significantly outperforms the existing approaches with nested arrays, and its output SINR is almost equal to the optimal value across a wide range of SNR.

REFERENCES

[1] J. Li and P. Stoica, *Robust Adaptive Beamforming*. New York, NY, USA: Wiley, 2005.
[2] X. Wang, L. Wan, M. Huang, C. Shen, and K. Zhang, "Polarization channel estimation for circular and non–circular signals in massive MIMO systems," *IEEE J. Sel. Top. Signal Process.*, vol. 13, no. 5, pp. 1001–1016, Sep. 2019.
[3] L. Wan, L. Sun, X. Kong, Y. Yuan, K. Sun, and F. Xia, "Task–driven resource assignment in mobile edge computing exploiting evolutionary computation," *IEEE Wireless Commun.*, vol. 26, no. 6, pp. 94–101, Dec. 2019.
[4] S. A. Vorobyov, "Principles of minimum variance robust adaptive beamforming design," *Signal Process.*, vol. 93, no. 12, pp. 3264–3277, Dec. 2013.
[5] B. Carlson, "Covariance matrix estimation errors and diagonal loading in adaptive arrays," *IEEE Trans. Aerosp. Electron. Syst.*, vol. 24, no. 4, pp. 397–401, Jul. 1988.
[6] D. Feldman and L. Griffiths, "A projection approach for robust adaptive beamforming," *IEEE Trans. Signal Process.*, vol. 42, no. 4, pp. 867–876, Apr. 1994.
[7] S. Vorobyov, A. Gershman, and Z.-Q. Luo, "Robust adaptive beamforming using worst-case performance optimization: A solution to the signal mismatch problem," *IEEE Trans. Signal Process.*, vol. 51, no. 2, pp. 313–324, Feb. 2003.
[8] J. Li, P. Stoica, and Z. Wang, "On robust capon beamforming and diagonal loading," *IEEE Trans. Signal Process.*, vol. 51, no. 7, pp. 1702–1715, Jul. 2003.
[9] S. Vorobyov, A. Gershman, Z.-Q. Luo, and N. Ma, "Adaptive beamforming with joint robustness against mismatched signal steering vector and interference nonstationarity," *IEEE Signal Process. Lett.*, vol. 11, no. 2, pp. 108–111, Feb. 2004.
[10] A. Hassanien, S. A. Vorobyov, and K. M. Wong, "Robust adaptive beamforming using sequential quadratic programming: An iterative solution to the mismatch problem," *IEEE Signal Process. Lett.*, vol. 15, pp. 733–736, 2008.
[11] J. Yang, X. Ma, C. Hou, and Y. Liu, "Automatic generalized loading for robust adaptive beamforming," *IEEE Signal Process. Lett.*, vol. 16, no. 3, pp. 219–222, Mar. 2009.
[12] L. Du, J. Li, and P. Stoica, "Fully automatic computation of diagonal loading levels for robust adaptive beamforming," *IEEE Trans. Aerosp. Electron. Syst.*, vol. 46, no. 1, pp. 449–458, Jan. 2010.
[13] Z. L. Yu, Z. Gu, J. Zhou, Y. Li, W. Ser, and M. H. Er, "A robust adaptive beamformer based on worst–case semi–definite programming," *IEEE Trans. Signal Process.*, vol. 58, no. 11, pp. 5914–5919, Nov. 2010.
[14] J. P. Lie, W. Ser, and C. M. S. See, "Adaptive uncertainty based iterative robust capon beamformer using steering vector mismatch estimation," *IEEE Trans. Signal Process.*, vol. 59, no. 9, pp. 4483–4488, Sep. 2011.
[15] B. Liao, K. M. Tsui, and S. C. Chan, "Robust beamforming with magnitude response constraints using iterative second–order cone programming," *IEEE Trans. Antennas Propagat.*, vol. 59, no. 9, pp. 3477–3482, Sep. 2011.

[16] A. Khabbazibasmenj, S. A. Vorobyov, and A. Hassanien, "Robust adaptive beamforming based on steering vector estimation with as little as possible prior information," *IEEE Trans. Signal Process.*, vol. 60, no. 6, pp. 2974–2987, Jun. 2012.
[17] F. Huang, W. Sheng, and X. Ma, "Modified projection approach for robust adaptive array beamforming," *Signal Process.*, vol. 92, no. 7, pp. 1758–1763, Jul. 2012.
[18] Y. Gu and A. Leshem, "Robust adaptive beamforming based on interference covariance matrix reconstruction and steering vector estimation," *IEEE Trans. Signal Process.*, vol. 60, no. 7, pp. 3881–3885, Jul. 2012.
[19] B. Liao, S.-C. Chan, and K.-M. Tsui, "Recursive steering vector estimation and adaptive beamforming under uncertainties," *IEEE Trans. Aerosp. Electron. Syst.*, vol. 49, no. 1, pp. 489–501, Jan. 2013.
[20] H. Ruan and R. C. De Lamare, "Robust adaptive beamforming using a low–complexity shrinkage–based mismatch estimation algorithm," *IEEE Signal Process. Lett.*, vol. 21, no. 1, pp. 60–64, Jan. 2014.
[21] Y. Gu, N. A. Goodman, S. Hong, and Y. Li, "Robust adaptive beamforming based on interference covariance matrix sparse reconstruction," *Signal Process.*, vol. 96, pp. 375–381, Mar. 2014.
[22] L. Huang, J. Zhang, X. Xu, and Z. Ye, "Robust adaptive beamforming with a novel interference-plus-noise covariance matrix reconstruction method," *IEEE Trans. Signal Process.*, vol. 63, no. 7, pp. 1643–1650, Apr. 2015.
[23] Y. Zhang, Y. Li, and M. Gao, "Robust adaptive beamforming based on the effectiveness of reconstruction," *Signal Process.*, vol. 120, pp. 572–579, Mar. 2016.
[24] H. Ruan and R. C. De Lamare, "Robust adaptive beamforming based on low–rank and cross–correlation techniques," *IEEE Trans. Signal Process.*, vol. 64, no. 15, pp. 3919–3932, Aug. 2016.
[25] M. Zhang, A. Zhang, and Q. Yang, "Robust adaptive beamforming based on conjugate gradient algorithms," *IEEE Trans. Signal Process.*, vol. 64, no. 22, pp. 6046–6057, Nov. 2016.
[26] B. Liao, C. Guo, L. Huang, Q. Li, G. Liao, and H. So, "Robust adaptive beamforming with random steering vector mismatch," *Signal Process.*, vol. 129, pp. 190–194, Dec. 2016.
[27] C. Zhou, Y. Gu, S. He, and Z. Shi, "A robust and efficient algorithm for coprime array adaptive beamforming," *IEEE Trans. Veh. Technol.*, vol. 67, no. 2, pp. 1099–1112, Feb. 2018.
[28] Z. Zheng, Y. Zheng, W.-Q. Wang, and H. Zhang, "Covariance matrix reconstruction with interference steering vector and power estimation for robust adaptive beamforming," *IEEE Trans. Veh. Technol.*, vol. 67, no. 9, pp. 8495–8503, Sep. 2018.
[29] Y. Huang and S. A. Vorobyov, "An inner socp approximate algorithm for robust adaptive beamforming for general-rank signal model," *IEEE Signal Process. Lett.*, vol. 25, no. 11, pp. 1735–1739, Nov. 2018.
[30] Z. Li, Y. Zhang, Q. Ge, and Y. Guo, "Middle subarray interference covariance matrix reconstruction approach for robust adaptive beamforming with mutual coupling," *IEEE Commun. Lett.*, vol. 23, no. 4, pp. 664–667, Apr. 2019.
[31] X. Zhu, Z. Ye, X. Xu, and R. Zheng, "Covariance matrix reconstruction via residual noise elimination and interference powers estimation for robust adaptive beamforming," *IEEE Access*, vol. 7, pp. 53262–53272, 2019.
[32] Y. Hou, H. Gao, Q. Huang, J. Qi, X. Mao, and C. Gu, "A robust capon beamforming approach for sparse array based on importance resampling compressive covariance sensing," *IEEE Access*, vol. 7, pp. 80478–80490, 2019.
[33] Y. Huang, M. Zhou, and S. A. Vorobyov, "New designs on MVDR robust adaptive beamforming based on optimal steering vector estimation," *IEEE Trans. Signal Process.*, vol. 67, no. 14, pp. 3624–3638, Jul. 2019.
[34] Z. Zheng, W.-Q. Wang, H. C. So, and Y. Liao, "Robust adaptive beamforming using a novel signal power estimation algorithm," *Digit. Signal Process.*, vol. 95, Dec. 2019, Art. no. 102574.
[35] Z. Zheng, T. Yang, W.-Q. Wang, and H. C. So, "Robust adaptive beamforming via simplified interference power estimation," *IEEE Trans. Aerosp. Electron. Syst.*, vol. 55, no. 6, pp. 3139–3152, Dec. 2019.
[36] X. Zhu, X. Xu, and Z. Ye, "Robust adaptive beamforming via subspace for interference covariance matrix reconstruction," *Signal Process.*, vol. 167, Art. no. 107289, Feb. 2020.
[37] Z. Zheng, T. Yang, W.-Q. Wang, and S. Zhang, "Robust adaptive beamforming via coprime coarray interpolation," *Signal Process.*, vol. 169, Art. no. 107382, Apr. 2020.
[38] P. Pal and P. P. Vaidyanathan, "Beamforming using passive nested arrays of sensors," in *Proc. IEEE Int. Symp. Circuits Syst. (ISCAS)*, Paris, France, May 2010, pp. 2840–2843.
[39] Z. Zheng, W.-Q. Wang, Y. Kong, and Y. D. Zhang, "MISC array: A new sparse array design achieving increased degrees of freedom and reduced mutual coupling effect," *IEEE Trans. Signal Process.*, vol. 67, no. 7, pp. 1728–1741, Apr. 2019.
[40] R. Hoctor and S. Kassam, "The unifying role of the coarray in aperture synthesis for coherent and incoherent imaging," *Proc. IEEE*, vol. 78, no. 4, pp. 735–752, Apr. 1990.
[41] P. Pal and P. P. Vaidyanathan, "Nested arrays: A novel approach to array processing with enhanced degrees of freedom," *IEEE Trans. Signal Process.*, vol. 58, no. 8, pp. 4167–4181, Aug. 2010.
[42] K. Han and A. Nehorai, "Wideband Gaussian source processing using a linear nested array," *IEEE Signal Process. Lett.*, vol. 20, no. 11, pp. 1110–1113, Nov. 2013.
[43] K. Han and A. Nehorai, "Nested array processing for distributed sources," *IEEE Signal Process. Lett.*, vol. 21, no. 9, pp. 1111–1114, Sep. 2014.
[44] P. Alinezhad, S. R. Seydnejad, and D. Abbasi-Moghadam, "DOA estimation in conformal arrays based on the nested array principles," *Digit. Signal Process.*, vol. 50, pp. 191–202, Mar. 2016.
[45] J. Yang, G. Liao, and J. Li, "An efficient off-grid DOA estimation approach for nested array signal processing by using sparse Bayesian learning strategies," *Signal Process.*, vol. 128, pp. 110–122, Nov. 2016.
[46] C. Wen, G. Shi, and X. Xie, "Estimation of directions of arrival of multiple distributed sources for nested array," *Signal Process.*, vol. 130, pp. 315–322, Jan. 2017.
[47] Y. Wang, A. Hashemi-Sakhtsari, M. Trinkle, and B. W.-H. Ng, "Sparsity-aware DOA estimation of quasi-stationary signals using nested arrays," *Signal Process.*, vol. 144, pp. 87–98, Mar. 2018.
[48] F. Chen, J. Dai, N. Hu, and Z. Ye, "Sparse Bayesian learning for off-grid DOA estimation with nested arrays," *Digit. Signal Process.*, vol. 82, pp. 187–193, Nov. 2018.
[49] G. Qin, Y. D. Zhang, and M. G. Amin, "DOA estimation exploiting moving dilated nested arrays," *IEEE Signal Process. Lett.*, vol. 26, no. 3, pp. 490–494, Mar. 2019.
[50] Z. Zheng, M. Fu, W.-Q. Wang, S. Zhang, and Y. Liao, "Localization of mixed near–field and far–field sources using symmetric double–nested arrays," *IEEE Trans. Antennas Propag.*, vol. 67, no. 11, pp. 7059–7070, Nov. 2019.
[51] L. Yu, Y. Wei, and W. Liu, "Adaptive beamforming based on nonuniform linear arrays with enhanced degrees of freedom," in *Proc. TENCON IEEE Region 10 Conf.*, Macao, China, Nov. 2015, pp. 1–5.
[52] C.-L. Liu and P. P. Vaidyanathan, "Remarks on the spatial smoothing step in coarray MUSIC," *IEEE Signal Process. Lett.*, vol. 22, no. 9, pp. 1438–1442, Sep. 2015.
[53] J. Yang, G. Liao, and J. Li, "Robust adaptive beamforming in nested array," *Signal Process.*, vol. 114, pp. 143–149, Sep. 2015.
[54] J. Capon, "High-resolution frequency-wavenumber spectrum analysis," *Proc. IEEE*, vol. 57, no. 8, pp. 1408–1418, 1969.
[55] M. Grant, S. Boyd, and Y. Ye. (Jun. 2015). *CVX: MATLAB Software for Disciplined Convex Programming, Version 2.1*. [Online]. Available: http://cvxr.com/cvx

ZHI ZHENG (Member, IEEE) received the M.S. degree in electronic engineering and the Ph.D. degree in information and communication engineering from the University of Electronic Science and Technology of China (UESTC), Chengdu, China, in 2007 and 2011, respectively. From 2014 to 2015, he was an Academic Visitor with the Department of Electrical and Electronic Engineering, Imperial College London, U.K. Since 2011, he has been with the School of Information and Communication Engineering, UESTC, where he is currently an Associate Professor. His research interests include statistical and array signal processing, including direction finding, source localization, target tracking, sparse array design, robust adaptive beamforming, jammer suppression, compressive sensing, machine learning, and convex optimization, with applications to radars, sonars, navigation, wireless communications, and wireless sensor networks.

TONG YANG received the B.S. degree in communication engineering from the University of Electronic Science and Technology of China (UESTC), Chengdu, China, in 2016, where he is currently pursuing the M.S. degree in communication and information systems. His research interests include array signal processing, robust adaptive beamforming, the direction-of-arrival estimation and source localization, and signal processing for communications.

DI JIANG received the B.S. degree in electrical engineering from the Guilin University of Electronic Technology, Guilin, China, in 2004, and the M.E. and Ph.D. degrees in electromagnetic field and microwave technology from the University of Electronic Science and Technology of China (UESTC), Chengdu, China, in 2009 and 2014, respectively. From 2012 to 2013, he was an Academic Visitor with the Engineering Department, Cambridge University. Since 2014, he has been with the School of Information and Communication Engineering, UESTC, where he is currently an Associate Professor. His research interests include microwave and millimeter-wave technology, reconfigurable antenna technology, array signal processing for radars, and communications and microwave remote sensing.

WEN-QIN WANG (Senior Member, IEEE) received the B.S. degree in electrical engineering from Shandong University, Shandong, China, in 2002, and the M.E. and Ph.D. degrees in information and communication engineering from the University of Electronic Science and Technology of China (UESTC), Chengdu, China, in 2005 and 2010, respectively.

From 2005 to 2007, he was with the National Key Laboratory of Microwave Imaging Technology, Chinese Academy of Sciences, Beijing, China. From 2011 to 2012, he was a Visiting Scholar with the Stevens Institute of Technology, Hoboken, NJ, USA. From 2012 to 2013, he was a Hong Kong Scholar with the City University of Hong Kong, Hong Kong. From 2014 to 2016, he was a Marie Curie Fellow of the Imperial College London, U.K. Since 2007, he has been with the School of Information and Communication Engineering, UESTC, where he is currently a Professor and the Director of MultiDimensional Information Sensing and Processing Research Centre. His research interests include array signal processing and circuit systems for radars, communications, and microwave remote sensing. He was a recipient of the Marie Curie International Incoming Fellowship, the National Young Top-Notch Talent of the Ten-Thousand Talent Program Award, and the Hong Kong Scholar Fellowship. He is an editorial board member of four international journals.